Malaysian Journal of Chemistry, 2021, Vol. 23(2), 55-62
(Special Issue: *IKM Pahang Branch Online Symposium 2021 – Chemistry for Sustainable World*)

DNA-Assisted Stabilization of Graphene Sheets and Its Application as Supercapacitors Electrode

Yasin M. Y. Albarqouni[1], Gomaa A. M. Ali[2], Soon Poh Lee[1], Rahim Mohd-Hairul[1] and Kwok Feng Chong[1]*

[1]Faculty of Industrial Sciences & Technology, Universiti Malaysia Pahang, Gambang, 26300 Kuantan, Malaysia
[2]Chemistry Department, Faculty of Science, Al–Azhar University, Assiut, 71524, Egypt
*Corresponding author (e-mail: ckfeng@ump.edu.my)

This work reports on the formation of rGO/ssDNA composite by stabilization of rGO sheets in an aqueous solution containing ssDNA extracted from baker's yeast culture. The as-formed rGO/ssDNA composite was verified using spectroscopic and microscopic techniques, including Fourier transform infrared (FTIR), Raman, and photoluminescence (PL) spectroscopies, and field emission scanning electron microscopy~~e~~ (FESEM). Physical investigations showed the successful stabilization of rGO suspension by ssDNA for more than a month without the rGO sheets precipitating. The highly charged backbone of ssDNA comprising phosphate groups, nucleic-bases, and sugar molecules contributed to the rGO stabilization and this could be a potential electrode material for a charge storage supercapacitor. Electrochemical investigations confirmed the electrochemical double-layer capacitance behavior of rGO/ssDNA composite in KOH electrolyte, where a nearly 2-fold capacitance enhancement was observed compared to pure rGO. The oxygen residues on ssDNA were shown to contribute to the electrochemically active surface area of rGO/ssDNA. By virtue of the approach simplicity of its preparation and its being environmentally benign, ~~it~~ the proposed material can be considered as a promising candidate for practical applications ~~of~~ as a bio-supercapacitor~~s~~ after further processing.

Key words: DNA; graphene; bio-supercapacitor

Received: November 2020; Accepted: January 2021

DNA, which was reported years ago as the main component responsible for storing, coding, and preserving genetic information, is currently studied in different disciplines, including material science, due to its outstanding chemistry enrichment [1,2]. The diversity of DNA-based applications in material science expanded to include single-strand nanowire to a highly ordered structure based on DNA origami [3]. The chemical functionalities endow DNA the ability to work as a template for metal~~s~~ growth [4], hydrogel template bio-based devices [5], or as an assisted material~~s~~ for carbon-based gel-like synthesis [6,7]. One of the attempts is to induce DNA in energy storage devices, including supercapacitors [8]. Supercapacitors have interests compared to batteries due to the low internal resistance and the high energy density it could provide [9]. In bio-systems, batteries have limitations due to the used chemicals and the prospective released chemical; for that, it is arguably to utilize energy storage systems as supercapacitors with a bio-based charge-storage materials due to its biocompatibility and safety [10]. The classification of supercapacitors is mainly due to its charge-storage mechanism based on the employed working electrodes. For instance, carbon-based materials are considered ideal electric double-layer capacitors (EDLC) where ions are adsorbed on the electrode/electrolyte interface [11].

On the other hand, pseudocapacitors, including metal oxides elucidate electrode/electrolyte interface redox reaction [12] or ion intercalation with active redox reaction [13]. Atomically thick layers of graphene synthesized from graphite reveal outstanding electric, thermal, and mechanical properties [14]. It is considered in the gold rush in electronic applications [15]. Even though it has outstanding characteristics, the sheets' self-aggregations, and the hydrophobicity limit its upgrade to the industrial level. Accessorized sheets of GO, with oxygen functional groups as epoxide and hydroxyl termed GO, can overcome the hydrophobicity due to its dual nature. GO holds potential for myriads of applications including energy applications as supercapacitors. Oxygen functionalities can ease various materials to physically attached or even form a strong bonding with the GO sheets, however, the oxygen contents challenge the ease of employment in electronic applications. A reduction and in situ functionalization of GO is a favorable idea to overcome GO insulation. Green reducing agents were reported to exhibit good performance for treating GO compared to toxic and corrosive traditional treatments such as hydrazine [16–18]. Graphene functionalization with other conducting materials enhance ions attraction on the supercapacitor system. Recent studies reported the

†Paper presented at the IKM Pahang Branch Online Symposium 2021 – Chemistry for Sustainable World

bio-functionalization of graphene with single-stranded DNA (ssDNA) to wrap and disperse carbon nanotubes (CNTs) and to assist in stabilizing graphene in aqueous dispersion to produce nanocomposites for prospective bio-based electronics applications [19,20]. DNA functionalize carbonaceous materials, including CNTs and GO, via non-covalent π-π stacking attachment due to the presence of purines and pyrimidine rings. GO and DNA are physically attached by π-π stacking due to the presence of aromatic rings in both structures. The dual nature of GO enable? it to form a stable colloidal dispersion in polar solvent, which facilitate the functionalization as well as the reduction to rGO sheets. In the meantime, the DNA backbone, which contains a phosphate-sugar complex, is oriented at? the outside interface of carbon materials, leading to the production of a hydrophilic dispersion. In this work, a modified green-approach was employed to produce a stable graphene dispersion functionalized with ssDNA to work as an energy storage supercapacitor device.

MATERIALS AND METHODS

Samples Preparation

Chemicals in this study were used without further purification. DNA used were obtained by a liquid phase extraction from baker's yeast following the Sambrook protocol [21]. GO material were synthesized using the Hummer's modified method as described in a previous report [22]. Graphite flakes were preoxidized by heating at 80 ºC in a mixture of sulfuric acid (H_2SO_4) potassium persulfate $K_2S_2O_8$, and phosphorus pentoxide P_2O_5 followed by full oxidization with potassium permanganate ($KMnO_4$) in the presence of H_2SO_4. The fully oxidized GO were washed by with a solution of HCl. Composite of rGO/DNA was prepared in a one-step reduction and functionalization process of GO with DNA. Typically, GO was incubated at 90 ºC with a DNA fragments pool, in a ratio of 1 to 4, in the presence of an equal weight of L-ascorbic acid as a reducing agent [6, 23]. The temperature used allows DNA to melt down into a single-stranded molecule, facilitating the attachment with GO with L-ascorbic acid assistings in the reduction process in the aqueous medium as previously reported.

Structural and Morphological Characterizations

DNA was characterized using Nano-dropper (NanoDrop™ 2000/2000c Spectrophotometer, Thermo fisher Co.). The concentration of DNA was evaluated by using the Sambrooks equation [24] (DNA concentration=A_{260}*Dilution factor*50). DNA was arrayed for 1 h in an agarose gel electrophoresis system (Bio-rad) using 80 V to qualitatively visualize DNA bands after hybridization with diamond orange dye (Diamond™ Nucleic Acid Dye-Promega Co.). Chemical groups of the synthesized GO and the reduced rGO were investigated using Fourier transform infrared spectroscopy (FTIR) in the wavelength range of 4000 to 400 cm^{-1}. Raman spectroscopy (InVia Reflex by Renishaw) with a 532 nm laser light source was conducted to investigate the structural changes of GO upon reduction and functionalization by observing the degree of sp^2 and sp^3 defects. Successful DNA functionalization was examined using photoluminescence spectroscopy (FLS1000) equipped with a xenon lamp with an excitation wavelength (λ_{ex}) of =278 nm). Morphological changes upon GO reduction was visualized using field emission scanning electron microscope (FESEM; JSM-7800 F by JEOL) at a voltage of 5.0 kV.

Electrochemical Characterizations

Electrochemical characteristics of rGO/ssDNA composite were investigated and compared with rGO in the three-electrode system (3ES) by applying different electrochemical techniques, including cyclic voltammetry (CV) and electrochemical impedance spectroscopy (EIS). Typically, 3ES consists of the working electrode (glassy carbon electrode) of the active material, Ag/AgCl (CH Instruments) as a reference electrode, and platinum (Pt) wire (CH Instruments) as a counter electrode. The electrochemical data were collected using an electrochemical workstation (AUTOLAB PGSTAT30, Netherlands) equipped with a frequency response analyzer.

RESULTS AND DISCUSSION

Structural and Morphological Characterizations

The purity of DNA, determined by calculating the ratio of A_{260} to A_{280}, was found to be about 1.75, which is very close to the ideal value for pure genomic DNA [25]. Extracted DNA was arrayed using a gel electrophoresis system, the result of which is as shown in Figure 1a. The extracted DNA seems to be fragmented, as represented in lanes 1 and 2. Genomic dsDNA shows a clear band in lane 3 with about 2.1 kbp. Structural investigation of the synthesized GO was observed by determining the oxygenated functional groups, after the oxidation process, using FTIR, the result of which is shown in Figure 1b. GO showeds four main peaks at 1050, 1219, 1400, and 1730 cm^{-1}, reflecting the sp^3 C–O (alkoxy) stretching peak, epoxy stretching vibration, C–H, and carbonyl group C=O bending, respectively [26,27]. Compared to the GO spectrum, the rGO showed slight spectral changes. The previously mentioned peaks in the GO spectrum disappeared upon incubation with L-ascorbic acid. The elimination of the oxygen functionalities could be attributed to the reduction reaction in the presence of L-ascorbic acid. Pure GO and rGO showed prominent peaks at 1637, and 3440 cm^{-1}, which were assigned to the C=C stretching vibration, and O-H stretching, respectively [27,28]. Raman spectroscopy gave valuable information about

the reduction process of GO and the functionalization of DNA to GO sheets. In general, Raman spectroscopy is conducted to study sp^3 and sp^2 disorders in the carbon-based materials [29,30], where a distinct pattern of carbonaceous materials can be reported by observing the D and G peaks. The D peak refers to the breathing mode of κ-point phonons of A_{1g} symmetry while the G peak refers to the first-order scattering of E_{2g} phonon of sp^2 carbon atoms. By investigating the intensity ratio of (I_D/I_G), valuable information about the distance between defect sites can be obtained, where the increment of the mean distance between two defects comes with an increment of I_D/I_G ratio. As shown in Figure 1c, both GO and rGO/ssDNA samples showed D and G peaks. Interestingly, the calculated I_D/I_G ratio of GO demonstrated~~s~~ a significant variation compared to that of rGO/ssDNA, where the former ratio is 0.89, while the latter is 1.13, indicating lower defect sites compared with GO. It is well known that upon the oxidation process of graphite flakes, higher defect sites can be assigned, which could be observed by the lower I_D/I_G. In contrast, the reduction of GO functional groups can restore the sp^2 carbon network, which reduces defect sites, and can be observed by the increment of the I_D/I_G ratio. Raman spectroscopy was also employed to study the binding of DNA in carbon sheets. The tangential G band in both composites (1595 cm^{-1}) was found to be red-shifted by about (5 cm^{-1}) compared to pure GO (1600 cm^{-1}). This shifting is ~~arguably~~ attributed to the charge transfer from the nucleic acid chains to GO sheets [31]. Similar to the findings in GO/ssDNA hydrogel and the wrapped carbon nanotube with DNA, G band for both composite is shifted upon ~~the~~ DNA attachement [6,32]. The energy transfer between ssDNA and rGO due to the functionalization was validated by observing the PL spectra of rGO before and after incubation with ssDNA. As illustrated in Figure 1d, rGO showed a PL intensity of about 450 cps; however, after incubation with DNA, the intensity was about 4-fold~~s~~ lower than that of pure rGO. The quenching of PL intensity could be attributed to the charge transfer between rGO and ssDNA composite [33,34].

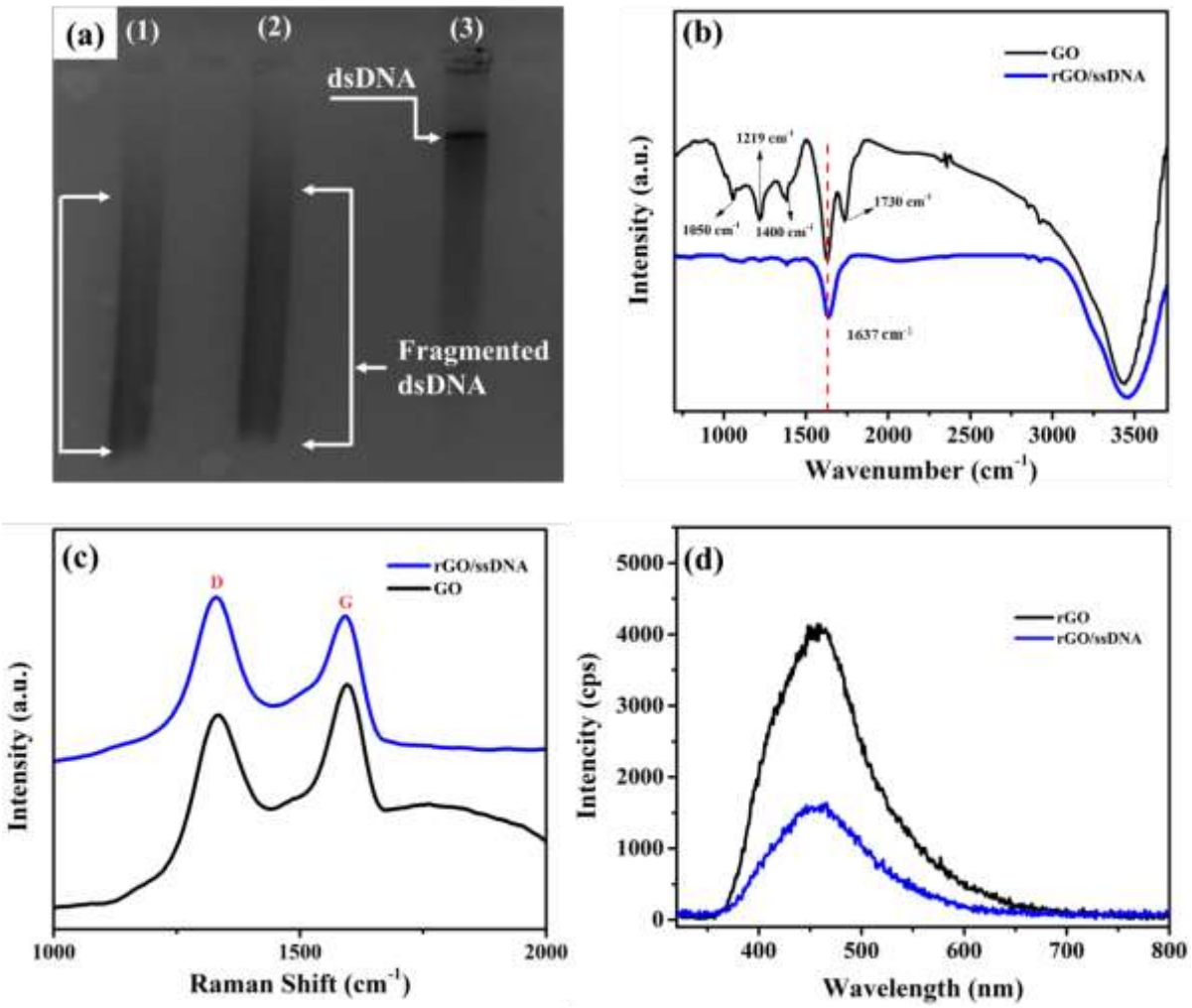

Figure 1. (a) Gel electrophoreses for dsDNA in lane 1, 2, and 3. GO and rGO/ssDNA characterizations using (b) FTIR, (c) Raman, and (d) photoluminescence spectra.

Figure 2. (a) Physical observation of GO and the solubilized rGO/ssDNA. (b) Microscopic investigation of rGO/ssDNA using FESEM in different magnifications.

The initial physical observation of the prepared composite showed a stable aqueous dispersion as expected even after 35 days, as illustrated in Figure 2a. The attachment of ssDNA to the reduced GO provides rGO with a hydrophilic surface, leading to solubilization of the reduced graphene oxide sheets in water. The observations mentioned above is a verification of the successful reduction of GO into rGO and its functionalization with ssDNA in different sequence lengths. The reduced and functionalized graphene oxide were visualized by FESEM using various magnifications. In Figure 2b, the rGO/ssDNA composite showed~~s~~ groovy sheets with thickness of about 0.42 nmMesopores can also be observed which has a direct impact on increasing the active surface area of the composite, leading to enhanced electrical properties [12].

Electrochemical Characterizations

The electrochemical characteristics of the pure rGO and rGO/ssDNA composites were determined using different electrochemical techniques, including CV and EIS using a three-electrode system in 1 M KOH electrolyte. The electrode~~'s~~ was prepared according to our previous report [35]. Figure 3 (a & b) shows the CV curves for rGO and rGO/ssDNA composites respectively.~~,~~ ~~b~~Both pure rGO and rGO/ssDNA ~~a~~ have semi-rectangular shapes with a ~~bit~~ slight deviation from the ideal shape in different scan rates (5, 10, 25, 50, 75, 100, 200~~)~~ mV s^{-1}). Such electrochemical shape? indicates the EDLC effect. The slight hump in the rGO/ssDNA composite is attributed to the surface redox reaction due to the presence of phosphorus and oxygen moieties in DNA [36]. It is well known that the higher the geometric area of the CV curve the higher the specific capacitance (C_S) in a given scan rate [37]. ~~B~~y comparing the CV curves for pure rGO and rGO/ssDNA as illustrated in Figure 3c, rGO/ssDNA electrode has a higher specific capacitance compared to rGO. A precise calculation of C_S can be obtained from the cyclic voltammetry curves in different scan rates (Figure 3d) by applying Equation 1 [38].

$$C_s = \int I dt/(m\Delta V) \quad (1)$$

where C_S is the average specific capacitance (F g^{-1}), I is the applied current (A), t is the time, m is the mass of the active electrode material (g), and V is the potential range of one sweep segment (V s^{-1}), respectively [39]. The calculated specific

capacitance for a single rGO/ssDNA electrode is about 97.3 F g^{-1}, which is 1.7-folds higher than the value for pure ~~(~~rGO (56.1 F g^{-1}) at 5 mV s^{-1}.~~;~~ ~~t~~The enhancement in specific capacitance confirms that ssDNA is successfully working~~ed~~ as a working electrode with rGO in a supercapacitor charge-storage system. The enrichment of phosphate groups, as well as the presence of nucleic bases Adenine (A), Guanine (G), Cytosine (C), and Thymine (T) in the ssDNA sequences, have a direct impact on facilitating the attraction of ions on the rGO/ssDNA electrode, leading to enhanced EDLC effect. Besides, the recorded specific capacitance of the rGO/ssDNA also shows a markedly larger value than that previously reported for DNA-based materials of? 60 F g^{-1} [8].

The charge mechanisms of the prepared electrodes were investigated by applying EIS at OCP in a frequency range from 100 kHz to 0.01 Hz at OCP in 1 M KOH as represented in Nyquist plots [40] ~~as~~ shown in Figure 4. Both rGO and rGO/ssDNA electrodes showed two distinct regions in the Nyquist plots; the first region is the semicircle in the high-frequency region, which indicates the ~~solution~~ electrolyte~~'s~~ solution resistance (R_S), and a near to vertical line which indicates the capacitive behavior. The distance between the Y-axis to the first point in the Nyquist plot indicates the charge-transfer resistance (R_{CT}) [41]. The equivalent circuit consists of a charge transfer resistance (R_{CT}), solution resistance (R_S), constant phase element (*CPE*) capacitor (*C*), and Warburg element (*W*). By comparing the fitted data of Nyquist plots for rGO and rGO/ssDNA composite, valuable information can be obtained. Both R_S & R_{CT} of the rGO/ssDNA electrode showed lower values compared to those of rGO. The semi-vertical line in the rGO/ssDNA electrode indicates a high EDLC effect compared to the EDLC effect of rGO. The enhancement of the capacitive effect in the rGO/ssDNA electrode is attributed to the increase of the electrochemical active surface area (S_E) due to the reduction of GO and the functionalization with sDNA~~,~~ which prevents the self-agglomeration of rGO sheets. An accurate calculation of the S_E for both electrodes was assigned from EIS by applying Equation 2 [42].

$$S_E = C_{dm}/C_d \quad (2)$$

where~~,~~ $C_{dm} = (2\pi f m Z'')^{-1}$, Z" is the imaginary impedance from Nyquist plots at the frequency (0.01 Hz) and C_d is a constant value of 20 µF cm^{-2} for carbonaceous materials [43]. The EIS fitted data for rGO, and rGO/ssDNA electrodes are tabulated as shown in Table 1. The results clearly shows the large increase in S_E of rGO/ssDNA as compared to that of rGO.

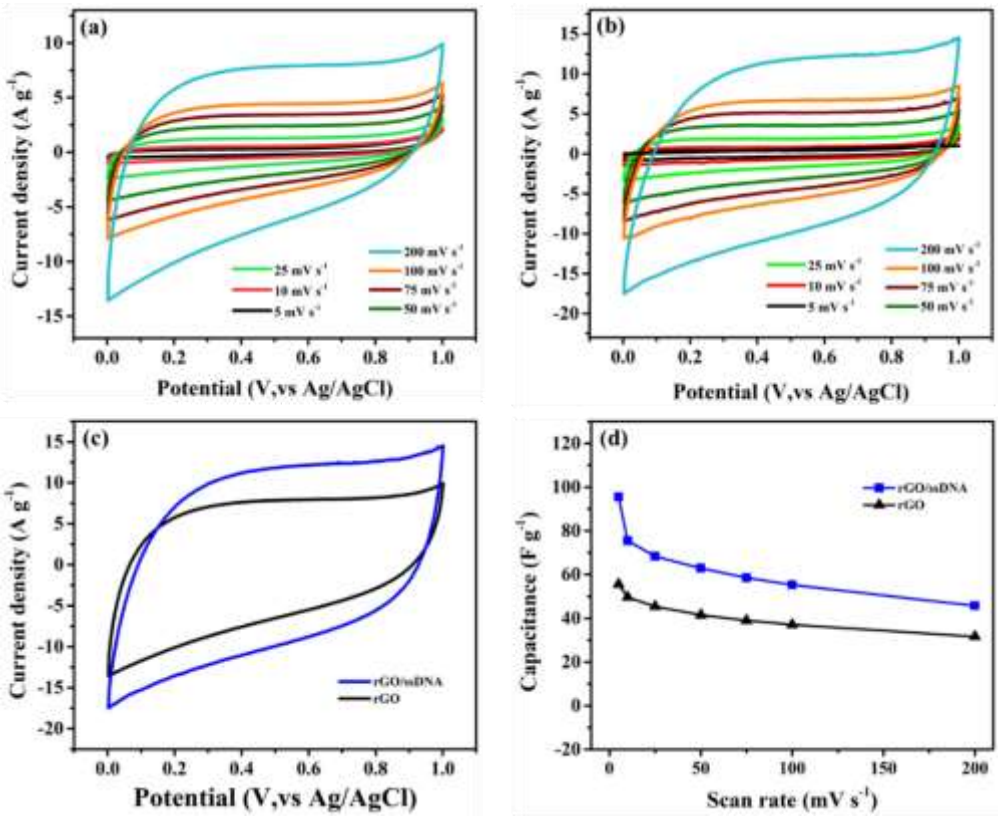

Figure 3. CV curves in different scan rates for (a) rGO and (b) rGO/ssDNA, and (c) a comparison between rGO and rGO/ssDNA at a scan rate of 200 mV s^{-1} in 1 M KOH. (d) Specific capacitance calculation for rGO and rGO/ssDNA electrodes at different scan rates.

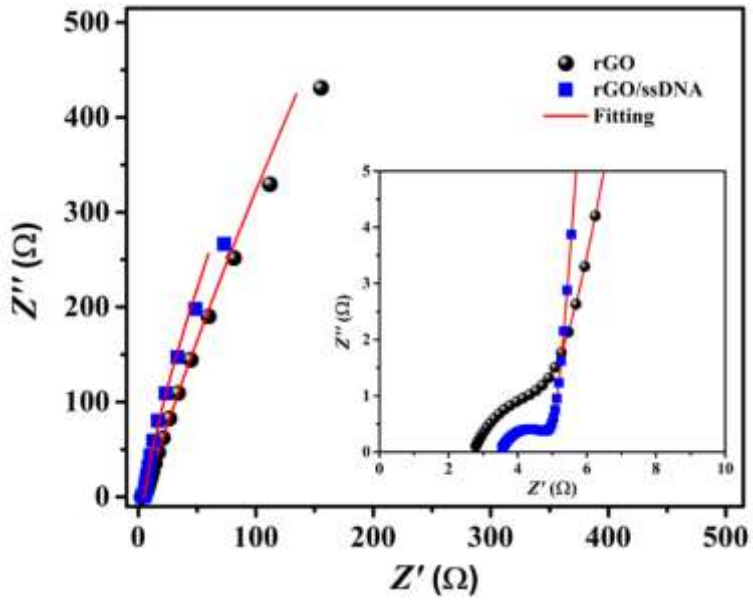

Figure 4. Nyquist plots for rGO and rGO/ssDNA composite in 1 M KOH.

Table 1. EIS fitted Data for rGO and rGO/ssDNA electrodes in 1 M KOH.

	R_S (Ω)	R_{CT} (Ω)	C (mF)	CPE (Ω^{-1} s^n)	W (Ω)	S_E (m^2 g^{-1})
rGO/ssDNA	3.39	2.46	0.619	0.110	0.056	501.9
GO	2.08	2.75	0.243	0.092	0.142	148.3

CONCLUSION

In conclusion, rGO/ssDNA composite was synthesized by a one-step simple wet-chemistry method. The synthesized composite showed a long-lasting stabilization in water due to the DNA backbone hydrophilicity. The successful synthesis of rGO/ssDNA was confirmed by using FTIR, Raman, and PL spectra. The reduced GO shows edgy thin layers. The rGO/ssDNA nanocomposite was utilized as an electrode material for supercapacitor energy storage. rGO/ssDNA showed almost ideal EDLC behavior with a nearly 2-folds capacitance compared with that of pure rGO in 1 M KOH electrolytes. The enhancement in capacitance is attributed to the increment of electrochemically active surface area due to the presence of nucleic acids, phosphate, and ribose sugar, leading to the easy adsorption~~b~~ of ions. The~~is~~ synthesis route used in this study provides a simple, green, and applicable way to synthesis DNA-carbon-based composites ~~to~~ can also be further used in other? applications.

ACKNOWLEDGMENT

The authors would like to acknowledge the funding from the Ministry of Education Malaysia in the form of grant number [RDU1901186:FRGS/1/2019/STG 07/UMP/02/6] and the Malaysia Toray Science Foundation grant RDU201502.

The authors declare that they have no conflict of interest.

REFERENCE

1. Burley, G. A., Gierlich, J., Mofid, M. R., Nir, H., Tal, S., Eichen, Y., Carell, T. (2006) Directed DNA metallization, *J. Am. Chem. Soc*., **128**, 1398–1399.

2. Liu, J., Geng, Y., Pound, E., Gyawali, S., Ashton, J. R., Hickey, J., Woolley, A. T., Harb, J. N. (2005) Metallization of branched DNA origami for nanoelectronic circuit fabrication, *ACS Nano*., **5**, 2240–2247.

3. Kwon, Y. W., Lee, C. H., Choi, D. H., Jin, J. Il (2009) Materials science of DNA, *J. Mater. Chem*., **19**, 1353–1380.

4. Xue, Y., Chen, T., Song, S., Kim, P., Bae, J. (2019) DNA-directed fabrication of $NiCo_2O_4$ nanoparticles on carbon nanotubes as electrodes

for high-performance battery-like electrochemical capacitive energy storage device, *Nano Energy*, **56,** 751–758.

5. Hur, J., Im, K., Hwang, S., Choi, B., Kim, S., Hwang, S., Park, N., Kim K. (2013) DNA hydrogel-based supercapacitors operating in physiological fluids, *Sci. Rep*., **3**.

6. Xu, Y., Wu, Q., Sun, Y., Bai, H., Shi, G. (2010) Three-dimensional self-assembly of graphene oxide and DNA into multifunctional hydrogels, *ACS Nano*., **4**, 7358–7362.

7. Zinchenko, A., Taki, Y., Sergeyev, V. G., Murata, S. (2014) DNA-assisted solubilization of carbon nanotubes and construction of DNA-MWCNT cross-linked hybrid hydrogels, *Nanomaterials*, **5**, 270–283.

8. Shin, S. R., Lee, C. K., So, I., Jeon, J. H., Kang, T. M., Kee, C., Kim, S. I., Spinks, G. M., Wallace, G. G., Kim, S. J. (2008) DNA-wrapped single-walled carbon nanotube hybrid fibers for supercapacitors and artificial muscles, *Adv. Mater*., **20**, 466–470.

9. Shao, Y., El-Kady, M. F., Sun, J., Li, Y., Zhang, Q., Zhu, M., Wang, H., Dunn, B., Kaner, R. B. (2018) Design and Mechanisms of Asymmetric Supercapacitors, *Chem. Rev*., **118**, 9233–9280.

10. Mosa, I. M., Pattammattel, A., Kadimisetty, K., Pande, P., El-Kady, M. F., Bishop, G. W., Novak, M., Kaner, R. B., Basu, A. K., Kumar, C. V., Rusling, J. F. (2017) Ultrathin Graphene–Protein Supercapacitors for Miniaturized Bioelectronics, *Adv. Energy Mater*., **7**, 1700358.

11. Ali, G. A. M., Yusoff, M. M., Chong, K. F., Makhlouf, S. A. (2015) Structural and electrochemical characteristics of graphene nanosheets as supercapacitor electrodes, *Rev. Adv. Mater. Sci.*, **41**, 35–43.

12. Marina, P. E., Ali, G. A. M., See, L. M., Teo, E. Y. L., Ng, E. P., Chong K. F. (2016) In situ growth of redox-active iron-centered nanoparticles on graphene sheets for specific capacitance enhancement, *Arab. J. Chem.*, **12**, 3883–3889.

13. Thalji, M. R., Ali, G. A. M., Algarni, H., Chong, K. F. (2019) Al^{3+} ion intercalation pseudocapacitance study of $W_{18}O_{49}$ nanostructure, *J. Power Sources*, **438**.

14. Geim, A. K., Novoselov, K. S. (2007) The rise of graphene, *Nat. Mater*., **6**, 183–191.

15. Zhang, L. L., Zhou, R., Zhao, X. S. (2010) Graphene-based materials as supercapacitor electrodes, *J. Mater. Chem*., **20**, 5983–5992.

16. Tai, M. J. Y., Liu, W. W., Khe, C. S., Hidayah, N. M. S., Teoh, Y. P., Voon, C. H., Lee, H. C., Adelyn, P. Y. P. (2018) Green synthesis of reduced graphene oxide using green tea extract, *AIP Conf. Proc*.

17. Haghighi, B., Tabrizi, M. A. (2013) Green-synthesis of reduced graphene oxide nanosheets using rose water and a survey on their characteristics and applications, *RSC Adv*., **3**, 13365–13371.

18. Kuila, T., Bose, S., Khanra, P., Mishra, A. K., Kim, N. H., Lee, J. H. (2012) A green approach for the reduction of graphene oxide by wild carrot root, *Carbon*, **50**, 914–921.

19. Patil, A. J., Vickery, J. L., Scott, T. B., Mann, S. (2009) Aqueous stabilization and self-assembly of craphene sheets into layered bio-nanocomposites using DNA, *Adv. Mater*., **21**, 3159–3164.

20. Zheng, M., Jagota, A., Strano, M. S., Santos, A. P., Barone, P., Chou, S. G., Diner, B. A., Dresselhaus, M. S., McLean, R. S., Onoa, G. B., Samsonidze, G. G., Semke, E. D., Usrey, M., Watts, D. J. (2003) Structure-Based Carbon Nanotube Sorting by Sequence-Dependent DNA Assembly, *Science*, **80 (302)**, 1545–1548.

21. Sambrook, J., Fritsch, E. F. (1989) Molecular cloning: a laboratory manual, *New York Cold Spring Harb. Lab. Press.*

22. Abu Bakar, N. H., Ali, G. A. M., Ismail, J., Algarni, H., Chong, K. F. (2019) Size-dependent corrosion behavior of graphene oxide coating, *Prog. Org. Coatings*, **134**, 272–280.

23. Cavallo, C., Agostini, M., Genders, J. P., Abdelhamid, M. E., Matic, A. (2019) A free-standing reduced graphene oxide aerogel as supporting electrode in a fluorine-free Li_2S_8 catholyte Li-S battery, *J. Power Sources*, **416**, 111–117.

24. Sambrook, J., Russel, W. (2000) Molecular Cloning, A Laboratory Manual, Cold Spring Harboc Lab. Press.

25. Olson, N. D., Morrow, J. B. (2012) DNA extract characterization process for microbial detection methods development and validation, *BMC Res. Notes*, **5**, 668.

26. Zhang, J., Yang, H., Shen, G., Cheng, P., Zhang,, J., Guo, S. (2010) Reduction of graphene oxide vial-ascorbic acid, *Chem. Commun*., **46**, 1112–1114.

27. Tanhaei, M., Mahjoub, A. R., Safarifard, V. (2019) Energy-efficient sonochemical approach

for the preparation of nanohybrid composites from graphene oxide and metal-organic framework, *Inorg. Chem. Commun.*, **102**, 185–191.

28. Lee, S. P., Ali, G. A. M., Algarni, H., Chong, K. F. (2019) Flake size-dependent adsorption of graphene oxide aerogel, *J. Mol. Liq.*, **277**, 175–180.

29. Martins Ferreira, E. H., Moutinho, M. V. O., Stavale, F., Lucchese, M. M., Capaz, R. B., Achete, C. A., Jorio, A. (2010) Evolution of the Raman spectra from single-, few-, and many-layer graphene with increasing disorder, *Phys. Rev. B - Condens. Matter Mater. Phys.*, **82**.

30. Milani, A., Tommasini, M., Russo, V., Bassi, A. L., Lucotti, A., Cataldo, F., Casari, C. S. (2015) Raman spectroscopy as a tool to investigate the structure and electronic properties of carbon-atom wires, *Beilstein J. Nanotechnol.*, **6**, 480–491.

31. Das, B., Voggu, R., Rout, C. S., Rao, C. N. R. (2008) Changes in the electronic structure and properties of graphene induced by molecular charge-transfer, *Chem. Commun.*, 5155–5157.

32. Erdem, A., Papakonstantinou, P., Murphy, H. (2006) Direct DNA hybridization at disposable graphite electrodes modified with carbon nanotubes, *Anal. Chem.*, **78**, 6656–6659.

33. Hamzah, M., Khenfouch, M., Srinivasu, V. V. (2017) The quenching of silver nanoparticles photoluminescence by graphene oxide: spectroscopic and morphological investigations, *J. Mater. Sci. Mater. Electron.*, **28**, 1804–1811.

34. Bi, S., Zhao, T., Luo, B. (2012) A graphene oxide platform for the assay of biomolecules based on chemiluminescence resonance energy transfer, *Chem. Commun.*, **48**, 106–108.

35. Ali, G. A. M., Yusoff, M. M., Shaaban, E. R., Chong, K. F. (2017) High performance MnO_2 nanoflower supercapacitor electrode by electrochemical recycling of spent batteries, *Ceram. Int.*, **43**, 8440–8448.

36. Krittayavathananon, A., Iamprasertkun, P., Sawangphruk, M. (2016) Enhancing the charge-storage performance of N-doped reduced graphene oxide aerogel supercapacitors by adsorption of the cationic electrolytes with single-stand deoxyribonucleic acid, *Carbon.*, **109**, 314–320.

37. Chee, W. K., Lim, H. N., Zainal, Z., Huang, N. M., Harrison, I., Andou, Y. (2016) Flexible Graphene-Based Supercapacitors: A Review, *J. Phys. Chem. C.*, **120**, 4153–4172.

38. Zhang, F., Cao, H., Yue, D., Zhou, Z. (2015) Graphene covalently modified by DNA G-base, *J. Phys. Chem. C.*, **117**, 3513–3519.

39. Zhao, J., Lai, H., Lyu, Z., Jiang, Y., Xie, K., Wang, X., Wu, Q., Yang, L., Jin, Z., Ma, Y., Liu, J., Hu, Z. (2015) Hydrophilic hierarchical nitrogen-doped carbon nanocages for ultrahigh supercapacitive performance, *Adv. Mater.*, **27**, 3541–3545.

40. Ali, G. A. M., Megiel, E., Cieciórski, P., Thalji, M. R., Romański, J., Algarni, H., Chong, K. F. (2020) Ferrocene functionalized multi-walled carbon nanotubes as supercapacitor electrodes, *J. Mol. Liq.*, 318.

41. Bhat, V. S., Jayeoye, T. J., Rujiralai, T., Sirimahachai, U., Chong, K. F., Hegde, G. (2020) Influence of surface properties on electrochemical supercapacitors utilizing Callerya atropurpurea pod derived porous nanocarbons: Structure property relationship between porous structures to energy storage devices , *Nano Sel.* 1, 226–243.

42. Ali, G. A. M., Lih Teo, E. Y., Aboelazm, E. A. A., Sadegh, H., Memar, A. O. H., Shahryari-Ghoshekandi, R., Chong, K. F. (2017) Capacitive performance of cysteamine functionalized carbon nanotubes, *Mater. Chem. Phys.*, **197**, 100–104.

43. Ali, G. A. M., Habeeb, O. A., Algarni, H., Chong, K. F. (2019) CaO impregnated highly porous honeycomb activated carbon from agriculture waste: symmetrical supercapacitor study, *J. Mater. Sci.*, **54**, 683–692.